Organic & Supramolecular Chemistry

Flower-Like Morphology of Naphthalene Diimides Containing *tetra*-L- and D-Alanine

Dada B. Shaikh,[a] Kerba S. More,[b] Mohammad Al Kobaisi,[c] Duong Duc La,[d] Sidhanath V. Bhosale,*[a] and Sheshanath V. Bhosale*[b]

Two structural isomers of naphthalene diimide (NDI) chromophores **NDI-3** and **NDI-4**, which are NDI imide position functionalised with four L-/D-alanine subunits. Density functional theory calculations revel that HOMO molecular orbital is localized on N-phenyl substituent and LUMO on NDI core. Further, the UV-vis, fluorescence measurements show that both the derivatives i.e. **NDI-3** and **NDI-4** exhibit changes in optical and photophysical properties with the addition of non-polar i.e. methylcyclohexane in chloroform as well as water in tetrahydrofuran. From these results, it is clear that the structural isomers **NDI-3** and **NDI-4** shows a significant solvatochromic effect, which ascribed to the aggregation effect via π-π stacking of NDI core along with hydrogen-bonding between alanine side chains. Scanning electron microscopy (SEM) and polarized optical microscopy images clearly demonstrate formation of flower like morphology in THF:H_2O and fiber nanostructure in $CHCl_3$:MCH for both **NDI-3** and **NDI-4**. Interestingly, only **NDI-4** in $CHCl_3$:MCH (4:6, v/v) solvent mixture produces rose-like flower microstructures.

1. Introduction

Development of nanostructure and microstructure morphology through supramolecular self-assembly has attracted much attention due to their potential applications in various fields such as materials and biology.[1,2] In self-assembly, the designing of small molecule organic building blocks makes a vital role to construct different morphology for fabrication of soft material. The noncovalent forces influences the morphology formation of various sizes and shape like nanospheres, nanotubular, nanofibre, nanowire, nano/micro flower, nano/microbelts, vesicles, micelle, etc. The formation of one, two and three dimensional (1D, 2D, and 3D) sophisticated structure has a different application from biology to material science. The balance between hydrogen bonding, π-π interaction, and van der Waal forces are important for the fabrication of the nanostructures of the chemical entity. The properties of self-assembled aggregates are different than that of the molecular building blocks.[3–12]

In general, supramolecular self-assembly of organic molecules may arranges in two specific ways: i) *H*-type aggregates, in which molecules arranged parallel (plane-to-plane stacking) and while the *J*-type aggregation molecule will arrange into head-to-tail fashion. Literature search revealed that the fiber and flower morphology have greatly useful in optoelectronics, catalysis, gas sensor, H_2O purifying agent, supercapacitor, photocatalytic agent, *etc.*[10,13–15] The fibril materials are also employed in tissue engineering, especially polymer fibril.[16] It is noted that stimuli responsive morphological changes of nanostructures due to the solvophobic effect are interesting. Such morphological changes are manipulated through change in solvent polarity and thermodynamic properties of the solvent. For the fabrication of different nanostructures, the designing of chemical structure and controlling of morphology are the challenging task. The different aromatic as well as aliphatic molecules such as pyrene, perylene diimides, tetraphenylethylene, diketopyrrolopyrrole, D-xyloside, L-rhamnose are utilized for the fabrication of nanostructures *via* self-assembly.[17–19]

It is well known that naphthalene diimides (NDIs)[20] are widely used building blocks for the fabrication of different nanostructures such as nanofibers,[21] nanotubes,[22] nanoflowers[23] and chiral materials.[24] NDIs are π-conjugated planar aromatic compound exhibiting n-type semiconducting properties and are employed in OFETs,[25] OLEDs[26] and solar cell[27] applications. In our previous work we have developed a series of chiral NDI derivatives and studied their self-assembly behaviour.[28] Thus in continuation of our work, herein, we designed NDI derivatives with four amino acid head groups to examine the influence of the nature of amino acids. We have newly synthesized amino acid based NDIs, which are sub-

[a] *Dr. D. B. Shaikh, S. V. Bhosale*
Polymers and Functional Materials Division
CSIR-Indian Institute of Chemical Technology
Hyderabad-500007, Telangana, India
E-mail: bhosale@iict.res.in
[b] *Mr. K. S. More, Prof. Dr. S. V. Bhosale*
School of Chemical Sciences
Goa University, Taleigao Plateau, Goa 403206 India
E-mail: svbhosale@unigoa.ac.in
[c] *Dr. M. A. Kobaisi*
School of Science, Faculty of Science, Engineering and Technology, Swinburne University of Technology, Hawthorn, Victoria 3122 Australia
[d] *Dr. D. D. La*
Institute of Chemistry and Materials, 17 Hoang Sam, Cay Giay, Hanoi, Vietnam

Supporting information for this article is available on the WWW under https://doi.org/10.1002/slct.202003108

stituted with four L-alanine (NDI-3) and D-alanine (NDI-4) (Figure 1). As expected that NDI-3 and NDI-4 led to the formation of various types of morphologies *via* amide H-bonding between alanine subunits along with π-π stacking of the NDI core. It was found that NDI-3 and NDI-4 exhibits fiber and flower-like assembled nanostructure formation in $CHCl_3$: MCH and THF:H_2O, respectively.

2. Results and Discussion

2.1. Synthesis and Characterization

Herein, we synthesized two derivatives of NDI having four amide bonds (Scheme S1). The commercially available NDA was treated with 5-aminoisophthalic acid in glacial acetic acid at 120 °C for 24 h. After the completion of reaction, the crude product was crystallized in dimethylformamide (DMF).[29] Furthermore, the synthesis of (2S,2′S,2″S,2‴S)-tetramethyl 2,2′,2″,2‴-((5,5′-(1,3,6,8-tetraoxobenzo[lmn][3,8]phenanthroline-2,7 (1H,3H,6H,8H)-diyl)bis (isophthaloyl)) tetrakis (azanediyl)) tetrapropanoate (NDI-3) achieved *via* amide coupling reaction between 5,5′-(1,3,6,8-tetraoxobenzo[lmn] [3,8]phenanthroline-2,7(1H,3H,6H,8H)-diyl)diisophthalic acid **1** and L-alanine methylester **4** in dry DMF using amide coupling reagent 1-ethyl-3(3-dimethylaminopropyl) carbodiimide hydrochloride (EDC.HCl), 1-hydroxybenzotriazole hydrate (HOBt) and *N,N*-diisopropylethylamine (DIPEA) for 24 h at room temperature. The structure of NDI-3 was confirmed by using analytical tools such as FT-IR, ^{1}H NMR, ^{13}C NMR and high resolution mass spectrometer.

As illustrated in ESI Figure S1, FT-IR spectra was employed to detect the functional groups of compound NDI-3, the peaks located at about 1670 cm^{-1}, 1716 cm^{-1} and 1741 cm^{-1} are ascribed to imide, amide and ester groups, respectively. Whereas, the aromatic C–H stretching frequency peak appeared at 2952 cm^{-1}. ^{1}H NMR spectra of NDI-3 was measured (ESI Figure S2). The chiral proton peak appeared at 4.78 ppm as quartet, at 3.78 ppm as singlet and 1.51 ppm as doublet for methoxy-methyl and methyl protons, respectively. As showed in ESI Figure S3, ^{13}C NMR the characteristic peak appeared at 172 ppm, 165 ppm and 162 ppm for ester, amide and imide –C=O carbons, respectively. As seen in ESI Figure 4, the structure of NDI-3 was confirmed by HRMS spectrum with 935.2730 $[M]^+$ and 957.2549 $[M+Na]^+$ ion peaks. Moreover, the synthesis of (2R,2′R,2″R,2‴R)-tetramethyl-2,2′,2″,2‴-((5,5′-(1,3,6,8-tetraoxobenzo[lmn][3,8] phenanthroline-2,7(1H,3H,6H,8H)-diyl)bis(isophthaloyl))tetrakis (azanediyl)) tetrapropanoate (NDI-4) was achieved utilizing the same reaction strategy like NDI-3. In order to confirm the structure of NDI-4, we employed spectroscopic techniques such as FT-IR, ^{1}H NMR, ^{13}C NMR, and HRMS spectrometer. ESI Figure S5 shows the stretching vibration frequency of –C=O of imide, amide and ester groups appeared at 1741 cm^{-1}, 1718 cm^{-1} and 1671 cm^{-1}, respectively. As illustrated in ESI Figure S6, ^{1}H NMR spectra of NDI-4 shows the distinguishable peak for chiral proton at 4.80 ppm as quartet and the methyl proton and methoxy-methyl proton appeared at 1.54 ppm and 3.79 ppm, respectively. In ^{13}C NMR, the peaks for carbonyl carbon appeared at 173 ppm, 165 ppm and 162 ppm corresponds to ester, amide, and imide carbonyl carbon, respectively (ESI Figure S7). Finally he structure of the compound NDI-4 was confirmed through HRMS spectrometer, the calculated molecular weight for $C_{46}H_{42}N_6O_{16}$ is 935.2739 and found 935.2730 $[M]^+$ and 957.2549 $[M+Na]^+$ shown in ESI Figure S8.

2.2. UV-vis Absorption Properties

The aggregation properties of NDI-3 and NDI-4 was characterized by UV-vis electronic absorption spectroscopy. UV-vis spectra of NDI-3 (1×10^{-5} M) in neat chloroform exhibited two absorption maxima at 380 nm, 360 nm along with a shoulder peak at 342 nm (Figure 2A). These peaks are originated from

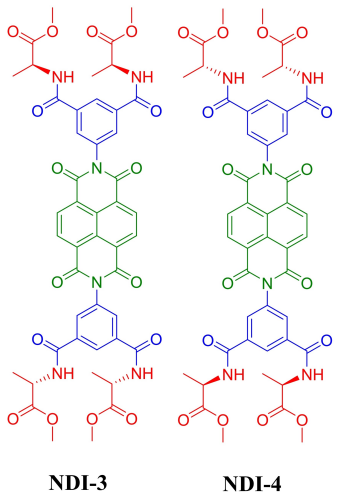

Figure 1. The molecular structures of the NDI-3 and NDI-4; L- and D-alanine derivative enantiomers.

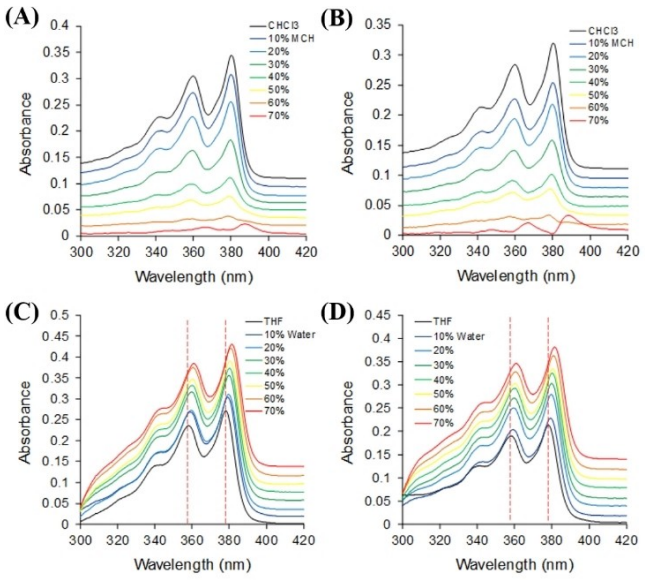

Figure 2. UV-vis absorption of (A) NDI-3, (B) NDI-4 in $CHCl_3$:MCH and (C) NDI-3, (D) NDI-4 in THF:H2O.

the π-π* transition. With the addition of MCH, the UV-vis changes of NDI-3 in $CHCl_3$ was monitored. Upon gradual addition of MCH proportion, NDI-3 shows decrease in absorption peak intensity at 342 nm, 360 nm and 380 nm, indicating the aggregation of NDI moiety *via* π-π stacking of NDI core. As illustrated in Figure 2B, similar trend i. e. decrease in absorption peak intensity was observed for NDI-4 in $CHCl_3$ with the addition of MCH (0-70%) and stabilized there. Thus, in both cases when we move from polar to more non-polar solvent system the absorption peak intensity was decreased quantitatively. These changes in absorption peak intensity of NDI-3 and NDI-4 were ascribed to the aggregation effect *via* π-π stacking in varying percentage of $CHCl_3$: MCH system.

In order to further verify the effect of more polar solvent on absorption properties of NDI-3 and NDI-4, UV-spectral measurements in THF and THF:H_2O solvent mixtures were recorded. As shown in Figure 2C, NDI-3 in THF solution exhibits well-resolved absorption maxima at 380 nm, 360 nm with shoulder peak at 342 nm. The absorption peaks at 380 nm, 360 nm are due to the $S_0 \rightarrow S_1$ transition. Furthermore, we performed titration experiments with the addition of different volume ratios of H_2O in THF. The addition of H_2O (0-70%) in THF solution, the absorption peak intensities of NDI-3 and NDI-4 decreased due to the π-π stacking of NDI core. Herein, we presume that the π-π staking effect of NDI aromatic core increased due to squeeze of H_2O from the hydrophobic core of NDI. Furthermore, the amide hydrogen bonding was involved in self-assembly formation. As shown in Figure 2D, the changes in UV-vis absorption intensity of NDI-4 with the addition of H_2O into THF were almost similar to that of NDI-3 system. Furthermore, fluorescence spectroscopy technique was employed to understand the aggregation behaviour of the compounds NDI-3 and NDI-4 in solution.

2.3. Fluorescence Emission Properties

The solvent effect on aggregation properties of NDI-3 and NDI-4 were examined by employing fluorescence emission spectrofluorophotometer measurements. The same concentration solution (1×10^{-5} M) was employed for emission to investigate the aggregation behavior of molecules in two solvent mixtures such as $CHCl_3$:MCH and THF:H_2O. As shown in Figure 3A, upon excitation at 355 nm (λ_{ex}), NDI-3 in neat $CHCl_3$ solution exhibited two prominent peaks at 410 nm, 430 nm and a shoulder peak at 460 nm. With the addition of MCH, the titration experiments were performed to get detail insight into aggregation behaviour of NDI-3. In the fluorescence emission experiments, addition of 10%, 20% and 30% MCH to $CHCl_3$ solution of NDI-3, shows no significant spectral changes. Further addition of MCH (40-90%) showed decrease in emission peak intensity with small blue shift. Moreover, the addition of 90% MCH, exhibit quantitative quenching of emission peaks. As shown in Figure 3B, NDI-4 in $CHCl_3$ exhibits two peaks at 410 nm and 430 nm with shoulder peak at 460 nm. In order to investigate the non-polar solvent effect on aggregation properties of NDI-4, we carried out titration experiments with the addition of MCH (0-90%). The addition of

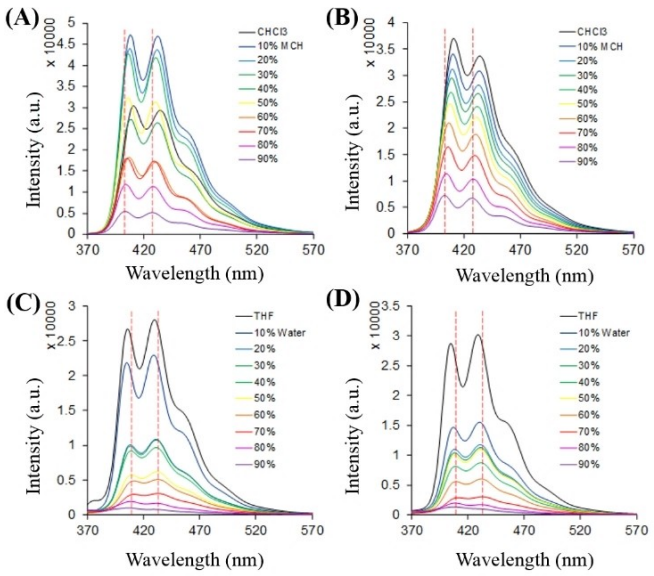

Figure 3. Fluorescence emission spectra of (A) NDI-3, (B) NDI-4 in $CHCl_3$:MCH and (C) NDI-3, (D) NDI-4 in THF:H_2O.

MCH (10-90%) showed gradual decrease in fluorescence peak intensity. The decrease in emission peak intensity of NDI-3 and NDI-4 were ascribed to π-π stacking of NDI core during the self-assembly formation. These results are consistent with those in the cases of UV-vis absorption.

In order to better confirm the effect of solvent polarity on aggregation behaviour of NDI-3 and NDI-4, emission titration experiments were performed in THF with the addition of H_2O (0-90%). As illustrated in Figure 3C and Figure 3D, upon excitation at 355 nm in THF, NDI-3 and NDI-4 exhibited the emission peaks at 430 nm, 405 nm along with shoulder peak at 452 nm. As shown in Figure 3C, with the addition of H_2O (10%) to THF solution of NDI-3, slight decrease in fluorescence intensity was observed. Furthermore, addition of H_2O (20%) clearly shows significant decrease in emission peak intensity. The emission intensity of NDI-3 were gradually decreasing with the addition of H_2O from 40–90%. However, the quantitative fluorescence quenching takes place in presence of 90% H_2O in THF. We further demonstrate the fluorescence spectral changes, with the addition of H_2O (0-90%) n THF and the results are depicted in Figure 3D. With the addition of 10% H_2O to NDI-4 in THF solution, the fluorescence intensity decreased significantly. Further addition of H_2O (20-90%) showed gradual decrease in emission peak intensity and reaches to zero at 90%. This indicates that NDI-3 and NDI-4 undergoes aggregation with more polar solvent addition. The quantitative quenching of fluorescence emission peaks are ascribed to the π-π stacking of NDI during self-assembly process. Herein, we presume that the hydrophobic interaction was increased with expel of H_2O. This leads to pronounced aggregation and quantitative fluorescence quenching of NDI-3 and NDI-4.

2.4. Field Emission Scanning Electron Microscopy (FE-SEM) Study

The self-assembled microstructure/nanostructure from NDI-3 and NDI-4 were studied by SEM measurements. NDI-4 produces fibrils structures along with rose-like flower microstructures from $CHCl_3$:MCH (4:6, *v/v* % ratio) as illustrated in Figure 4, however, NDI-3 produces only rectangular fibril network structures (Figure S9). Interestingly, both the NDI-3 and NDI-4 produces the irregular nanofiber, respectively as shown in ESI Figure S10. These nanofibers are several micrometer in length. We presume that the nonpolar solvent makes a crucial role in constructing the fiber-like morphology of aggregates in higher percentage of MCH. It clearly demonstrated that the MCH favored the hydrogen bonding along with π-π interaction between NDI core.

In order to gain detail insight of polar solvent effect, we investigated self-assembly of NDI-4 and NDI-3 in THF:H_2O (1:9, *v/v*% ratio) solvent mixture. In this solvent system both NDI-3 and NDI-4 produces flower-like supramolecular self-assembly formation as shown in Figure 5A and 5B, respectively. The size of these flowers are several micrometer. The arrangement of petals flower like aggregates of NDI-4 and NDI-3 are somewhat different. Herein, we presume that during aggregation H_2O squeezes out from the assembly due to hydrophobic nature of NDI core.

It is clear that the polarity of the solvent plays an important role during the formation of microstructure. It was observed that the formation of complex architecture mainly due to the hydrogen bonding and π-π stacking in both solvent systems. We can easily differentiate the aggregation of both the molecules NDI-3 and NDI-4 in different solvent due to the solvophobic effect. We have tried to study single X-ray crystallographic study but failed to obtain suitable crystal structure to see interactions, even tried various solvents (Table S1).

2.5. Polarize Optical Microscopy Study

The self-assembled nanostructures from the NDI-3 and NDI-4 were investigated by polarized microscopy measurements and are depicted in Figure 6A and Figure 6B, respectively. To systematically study the nature of the self-assembly formation, we varied the solvent mixing ratio. As seen in SEM imaging (Figure 5), polarize optical microscopy in THF:H_2O (1:9, *v/v* ratio), NDI-3 as well as NDI-4 led to microflower assembly formation, similar to results obtained in SEM imagining (Figure 5), respectively.

2.6. Dynamic Light Scattering Study (DLS)

The self-assembly of NDI-3 and NDI-4 in $CHCl_3$:MCH (1:9, *v/v*% ratio) and THF:H_2O (1:9, *v/v*% ratio) solution system were studied using DLS measurements (Figure 11). NDI-3 in $CHCl_3$:MCH (1:9, *v/v*% ratio) shows hydrodynamic size of 1500 nm (Figure S11A), whereas, NDI-4 gives peak at 500 nm (Figure S11C). As illustrated in Figure S11B and Figure S11D, in THF:H_2O (1:9, *v/v*% ratio) solution, NDI-3 exhibits hydrodynamic size of 100 nm and NDI-4 produces 400 nm size particles, respectively. It is observed that in solution the size of self-assembled nanostructures are smaller than on surface examined by SEM techniques. This may attributed to on surface solvent evaporation may lead to larger size nanostructures.

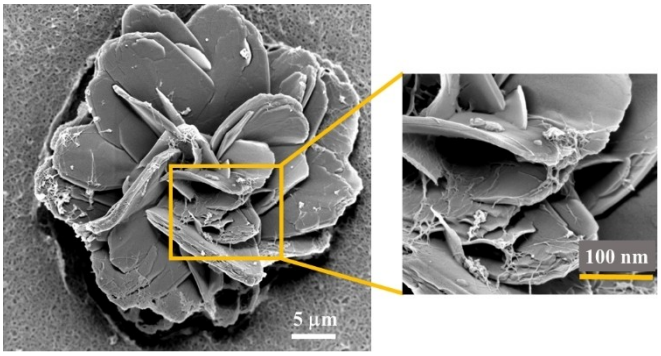

Figure 4. SEM micrographs of NDI-4 in $CHCl_3$:MCH (4:6, v/v% ratio) solution.

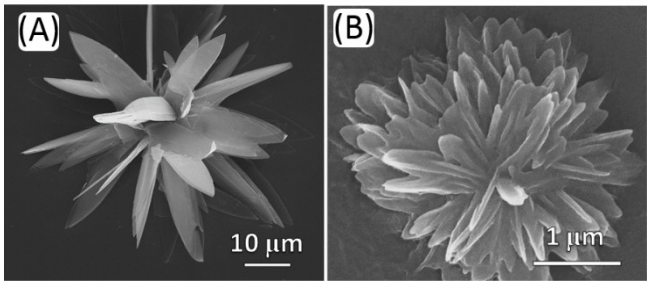

Figure 5. SEM images flower-like micrograph of (A) NDI-4 and (B) NDI-3 from THF:H_2O (1:9, v/v% ratio) mixture of solvents, respectively.

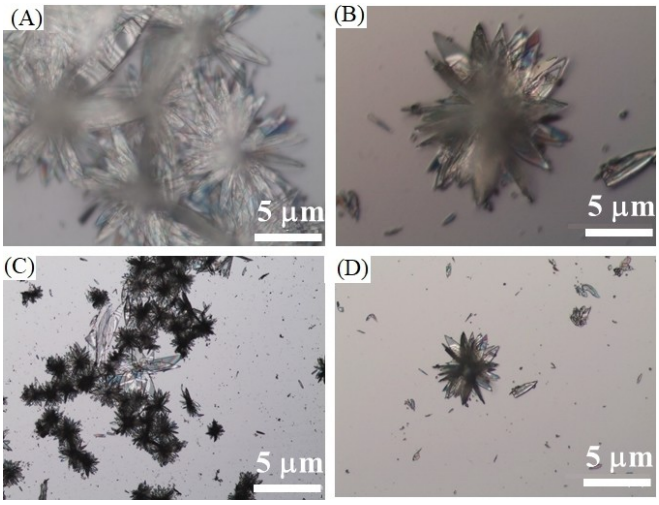

Figure 6. Light microscopy images of (A) NDI-3 and (B) NDI-4 deposited from 1:9 v/v% ratio THF:H_2O solution.

2.7. X-ray diffraction (XRD) Properties

The supramolecular self-assembly formation was further studied using X-ray diffraction measurements and the results are depicted in Figure 7. NDI-3 and NDI-4 does not show any XRD peak in its powder form. Whereas, the assembly of NDI-3 and NDI-4 exhibits clear diffraction peaks in THF:H_2O (1 : 9, *v/v*% ratio). These results suggest that the self-assembled material is crystalline in nature.

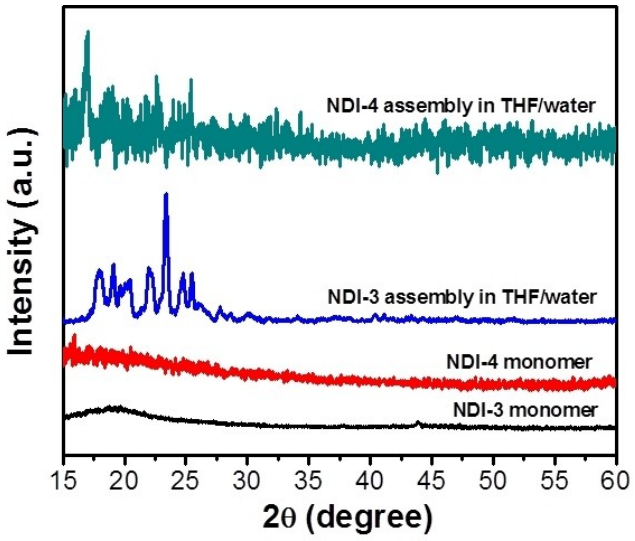

Figure 7. X-RD pattern in THF of NDI-3 (black line) and NDI-4 (red line) the blue line NDI-3 in THF:H_2O (1 : 9, v/v ratio) and green line NDI-4 THF:H_2O (1 : 9, v/v ratio).

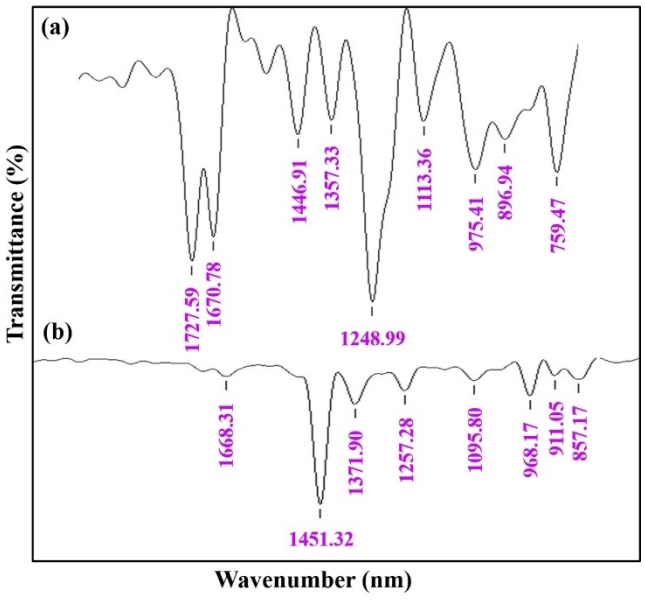

Figure 8. FT-IR spectra of NDI-3 in (a) $CHCl_3$ and (b) $CHCl_3$:MCH (1 : 9, *v/v* ratio) (1 : 9, *v/v* ratio).

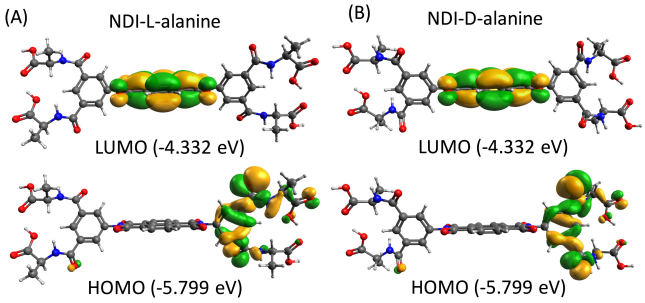

Figure 9. The frontier molecular orbitals HOMO and LUMO wave function and energy levels of (A) NDI-3 and (B) NDI-4 as calculated using ORCA 4.0 set of programs with DFT at BP86 def2-SVP def2/J D3BJ basis set.

2.8. Fourier Transform Infrared (FT-IR) Spectroscopy study

FT-IR spectra of NDI-3 in $CHCl_3$ and $CHCl_3$:MCH (1 : 9, *v/v* ratio) is illustrated in Figure 8. The absorption peaks at 1727 cm^{-1} and 1670 cm^{-1} can be assigned to the stretching vibration of the –C=O functional groups of ester and amide/imide of compound NDI-3 in $CHCl_3$. In $CHCl_3$:MCH (1 : 9, *v/v* ratio), the –C=O stretching vibration at 1727 cm^{-1} disappeared, while the associated absorption peak of ester –C=O intensity decreased with small shift of ~2 cm^{-1} (1668 cm^{-1}). The diminishing of absorption peak at 1727 cm^{-1} and decrease in peak intensity at 1670 cm^{-1} indicates assembly formation takes place *via* H-bonding. Therefore we conclude that the ester carbonyl group and amide carbonyl groups may associated through hydrogen bonding. The same trend was observed for the compound NDI-4, the absorption peaks at 1736 cm^{-1} and 1668 cm^{-1} in $CHCl_3$ are shifted to 716 cm^{-1} and 1655 cm^{-1} in $CHCl_3$:MCH (1 : 9, *v/v* ratio) as shown in ESI Figure S12. This clearly suggesting H-bonding takes place during self-assembly formation.

2.9. Density Functional Theory (DFT) Calculations

The *in vacuo* density functional theory (DFT) calculations were conducted using the ORCA 4.0 suit of programs.[29] The molecular structures were geometry optimized at BP86 def2-SVP def2/J D3BJ basis set DFT. Gauss-Sum 3.0 program[30] and Avogadro version 1.2.0[31] were used to build the molecular structures and process the results of ORCA calculations. The calculations showed a LUMO concentrated on the NDI core for both NDI derivative enantiomers, while the HOMO is concentrated on the N-substitutions (Figure 9). The energy gap between HOMO and LUMO for NDI-3 and NDI-4 found was 1.467 eV.

2.10. Theoretical Absorbance and Circular Dichroism Properties

As shown in Figures 10A–D, TD-DFT calculations were employed to estimate the theoretical absorption and circular dichroism (CD) spectra. For HOMO to LUMO excitation, TD-DFT results exhibit the absorption peaks at 360 nm (oscillator

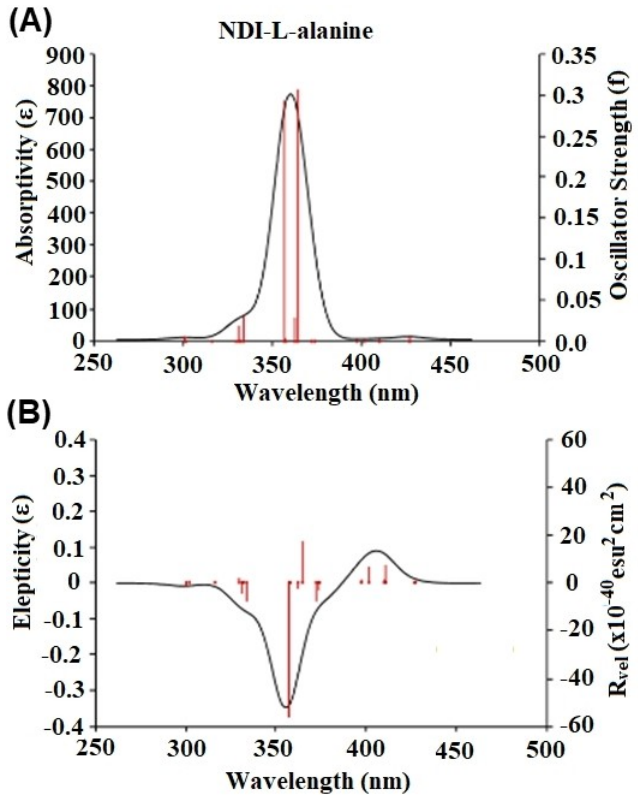

Figure 10. Simulated UV-vis absorption and CD spectra of NDI–L-Alanine (NDI-3) based on the first 20 electronic singlet excited states as calculated using TD-DFT at B3LYP def2-TZVP def2/J with RIJCOSX approximation level of theory with ORCA 4.0 set of programs and Gauss-Sum 3.0 program.

strength $f = 0.3$) for NDI-3 (Figure 10A) and NDI-4 (Figure S13A). The stimulated CD spectra exhibits -ve Cotton effect peak at 352 nm and +ve Cotton effect peak at 405 nm for NDI-3 (Figure 10B), whereas, for NDI-4, the +ve Cotton effect peak at 350 nm and -ve Cotton effect peak at 405 nm (Figure S13B). From these results we conclude that the NDI derivative NDI-3 shows different chirality than that of NDI-4.

Figure 11 (A–F) is direct visualization of the self-assembled microstructures shows unique mechanism of flower assembly with step-wise growth of 3-dimentional flower-like fractals of NDI-4 in THF-H_2O (1:9, v/v). The samples were prepared by evaporating the solvent mixture over 3 hours of the time and the SEM images were collected for the formation at various stages of growth of the same sample. As from the SEM images of Figure 5, it is clear that the NDI-4 probably assembled into a dimer which subsequently rearranges to grow the fractals and finally growth of flower observed in large surface (Figure 11G). It is also clear that 3-dimentioanl hierarchically self-assembled fractal formed from core or NDI with π-π-interactions along with stabilization of the structures by hydrogen-bonding. As lover volume of water content i.e. less than 80% in THF does not produces any decent flowers rather produces fibrils and also non polar solvents mixture such as $CHCl_3$-MCH at (1:9, v/v) produces fibril structures (Figure S10). Further, optical microscopy clearly supports formation of flower structures by solvent evaporation of both NDI-3 and NDI-4 in THF-H_2O ($f_w = 90\%$) solutions at room temperature (Figure 5). Similar flower like morphology of pentacyclic dihydroxy-triterpenoid betulin was reported by Bag *et al.*[23c] In which they observed flower like-assembly in three main steps: firstly formation of fiber followed by petals and finally flower assembly. However, in our study, we observed directly petal-like morphology which assembled into flower-like structures (Figure 11).

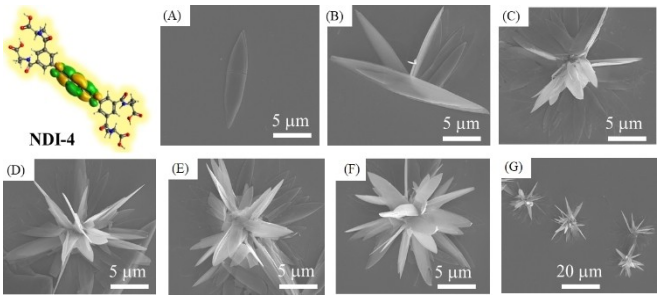

Figure 11. Step-by-step growth of the flower-like 3D fractal assembly deposited by solvent evaporation of THF-H_2O ($fw = 90\%$) solutions. Flower like assembly formation over 3 hrs time (A–F) and overall flower-like assembly growth at 20 μm scale shown in (G).

3. Conclusion

In this study, we demonstrated the self-assembly of naphthalene diimide bearing L- and D- alanine derivatives in various proportion of $CHCl_3$:MCH (1:9, v/v) and THF:H_2O (1:9, v/v) solution. The supramolecular self-assembled nanostructures such as nanofiber and microflower formation was achieved. The polarity of solvent plays a crucial role in nanostructure morphology formation. Herein, the delight balance between H-bonding and π-π stacking may trigger different type of morphology upon interaction with different solvent mixtures. In the present system π-conjugated NDI based molecular architecture is used. In the present NDI based system we observed directly petal like morphology which further assemble to form flowers. The designing of molecular structure is a helpful tool to fabricate the controlled morphology of aggregates.

Supporting Information

The details experimental for synthesis of molecules and their characterization ^{1}H NMR, ^{13}C NMR and IR spectra. Along with more SEM images, DLS analysis are available online.

Acknowledgements

SVB (IICT) is thankful to The Director CSIR-IICT for providing necessary facilities and financial support under the project P07. IICT Commun. No. IICT/Pubs./2020/008. DBS acknowledges the UGC for financial support under SRF. S.V.B. (GU) University Grant Commission (UGC) Faculty Research Program, New Delhi, India (F.4-5(50-FRP)(IV–Cycle)/2017(BSR)) for an award of Professorship

*and also acknowledges Council of Scientific & Industrial Research (**CSIR**), India for providing support, code No. 02(0357)/19/EMR-II.*

Conflict of Interest

The authors declare no conflict of interest.

Keywords: aggregation · flower-like morphology · naphthalene diimide · π-π-interactions · self-assembly

[1] L. Maggini, D. Bonifazi, *Chem. Soc. Rev.* **2012**, *41*, 211–241.
[2] Z. Chen, A. Lohr, C. R. Saha-Möller, F. Würthner, *Chem. Soc. Rev.* **2009**, *38*, 564–584.
[3] A. Ajayaghosh, V. K. Praveen, *Acc. Chem. Res.* **2007**, *40*, 644–656.
[4] D. González-Rodríguez, A. P. H. Schenning, *J. Chem. Mater.* **2011**, *23*, 310–325.
[5] D. Ghosh, *S. Chem. Commun.* **2016**, *52*, 6860–6872.
[6] V. K. Praveen, C. Ranjith, N. Armaroli, *Angew. Chem. Int. Ed.* **2014**, *53*, 365–368; *Angew. Chem.* **2014**, *126*, 373–376.
[7] H. Klauk, *Chem. Soc. Rev.* **2010**, *39*, 2643–2666.
[8] A. A. Virkar, S. Mannsfeld, Z. Bao, N. Stingelin, *Adv. Mater.* **2010**, *22*, 3857–3875.
[9] J. Zhang, H. Geng, T. S. Virk, Y. Zhao, J. Tan, C.-A. Di, W. Xu, K. Singh, W. Hu, Z. Shuai, Y. Liu, D. Zhu, *Adv. Mater.* **2012**, *24*, 2603–2607.
[10] F. Würthner, T. E. Kaiser, C. R. Saha-Möller, *Angew. Chem. Int. Ed.* **2011**, *50*, 3376–3410; *Angew. Chem.* **2011**, *123*, 3436–3473.
[11] H.-J. Jin, S. V. Fridrikh, G. C. Rutledge, D. L. Kaplan, *Biomacromolecules* **2002**, *3*, 1233–1239.
[12] S. Yagai, *Bull. Chem. Soc. Jap.* **2015**, *88*, 28–58.
[13] S. S. Babu, V. K. Praveen, A. Ajayaghosh, *Chem. Rev.* **2014**, *114*, 1973–2129.
[14] S. Yagai, T. Seki, T. Karatsu, A. Kitamura, F. Würthner, *Angew. Chem. Int. Ed.* **2008**, *47*, 3367–3371; *Angew. Chem.* **2008**, *120*, 3415–3419.
[15] X. Zhang, S. Rehm, M. M. Safont-Sempere, F. Würthner, *Nat. Chem.* **2009**, *1*, 623–629.
[16] A. Fertala, W. B. Han, F. K. Ko, *J. Biomed. Mater. Res.* **2001**, *57*, 48–58.
[17] W. Jiang, Y. Zhou, H. Geng, S. Jiang, S. Yan, W. Hu, Z. Wang, Z. Shuai, J. Pei, *J. Am. Chem. Soc.* **2011**, *133*, 1–3.
[18] R. Charvet, Y. Yamamoto, T. Sasaki, J. Kim, K. Kato, M. Takata, A. Saeki, S. Seki, T. Aida, *J. Am. Chem. Soc.* **2012**, *134*, 2524–2527.
[19] Y. Yamamoto, T. Fukushima, Y. Suna, N. Ishii, A. Saeki, S. Seki, S. Tagawa, M. Taniguchi, T. Kawai, T. Aida, *Science* **2006**, *314*, 1761–1764.
[20] M. Al Kobaisi, S. V. Bhosale, K. Latham, A. M. Raynor, S. V. Bhosale, *Chem. Rev.* **2016**, *116*, 11685–11796.
[21] L. Gonzalez, C. Liu, B. Dietrich, H. Su, S. Sproules, H. Cui, D. Honecker, D. J. Adams, E. R. Draper, *Commun. Chem.* **2018**, 1, 77.
[22] a) N. Ponnuswamy, A. R. Stefankiewicz, J. K. Sanders, G. D. Pantoş, *Top. Curr. Chem.* **2012**, *322*, 217–260; b) S. Y. Tu, S. H. Kim, J. Joseph, D. A. Modarelli, J. R. Parquette, *J. Am. Chem. Soc.* **2011**, *133*, 19125–19130.
[23] a) R. S. Bhosale, M. Al Kobaisi, S. V. Bhosale, S. Bhargava, S. V. Bhosale, *Sci. Rep.* **2015**, 5, 14609; b) R. S. Bhosale, D. D. La, S. D. Padghan, M. Al Kobaisi, L. A. Jones, S. V. Bhosale, S. V. Bhosale, *ChemistrySelect* **2017**, *2*, 10118–10122; c) B. G. Bag, S. S. Dash, *Langmuir* **2015**, *31*,13664–13672; d) S. M. Wagalgave, S. D. Padghan, M. Al Kobaisi, D. D. La, K. Bhamidipati, N. Puvvada, R. S. Bhosale, S. V. Bhosale, S. V. Bhosale, *New J. Chem.* **2020**, *44*, 18092–1810; e) S. V. Bhosale, M. Al Kibasis, R. W. Jadhav, L. A. Jones, *Chem. Rec.* 2020, DOI: tcr.202000129
[24] a) F. Salerno, J. A. Berrocal, A. T. Haedler, F. Zinna, E. W. Meijer, L. D. Bari, *J. Mater. Chem. C* **2017**, *5*3609–3615; b) X. Shang, I. Song, G. Y. Jung, W. Choi, H. Ohtsu, J. H. Lee, J. Y. Koo, B. Liu, J. Ahn, M. Kawano, S. K. Kwak, *Nat. Commun.* **2018**, *9*, 3933; c) M. Pandeeswar, H. Khare, S. Ramakumar, T. Govindaraju, *RSC Adv.* **2014**, *4*, 20154–20163.
[25] a) B.-L. Hu, K. Zhang, C. An, W. Pisula, M. Baumgarten, *Org. Lett.* **2017**, *19*, 6300–6303; b) Y. Zhang, D. Huan, C.-A. Di, D. Zhu, *Adv. Mater.* 2016, 28, 4549–4555.
[26] H. F. Higginbotham, P. Pander, R. Rybakiewicz, M. K. Etherington, S. Maniam, M. Zagorska, A. Pron, A. P. Monkman, P. Data, *J. Mater. Chem. C* **2018**, *6*, 8219–8225.
[27] a) J. Wang, X. Zhan, *Trends Chem.* **2019**, *1* (9), 869–881; b) P. S. Rao, A. Gupta, D. Srivani, S. V. Bhosale, A. Bilic, J. Li, W. Xiang, R. A. Evans, S. V. Bhosale, *Chem. Commun.* **2018**, *54*, 5062–5065; c) D. B. Shaikh, A. Ali Said, Z. Wang, P. S. Rao, R. S. Bhosale, A. M. Mak, K. Zhao, Y. Zhou, W. Liu, W. Gao, J. Xie, S. V. Bhosale, S. V. Bhosale, Q. Zhang, *ACS Appl. Mater. Interfaces* **2019**, *11*, 44487–44500.
[28] a) S. P. Goskulwad, M. Al Kobaisi, D. D. La, R. S. Bhosale, S. V. Bhosale, S. V. Bhosale, *Chem. Asian J.* **2018**, *13*, 3947–3953; b) S. P. Goskulwad, D. D. La, M. Al. Kobaisi, S. V. Bhosale, V. Bansal, A. Vinu, K. Ariga, S. V. Bhosale, *Sci. Rep.* **2018**, *8*, 11220.
[29] F. Neese, *WIREs Comput. Mol. Sci.* **2012**, *2*, 73–78.
[30] N. M. O'boyle, A. L. Tenderholt, K. M. Langner, *J. Comput. Chem.* 2008, 29 (5), 839–845.
[31] M. D. Hanwell, D. E. Curtis, D. C. Lonie, T. Vandermeersch, E. Zurek, G. R. Hutchison, *J. Cheminformatics* **2012**, *4*, 17.

Submitted: August 6, 2020
Accepted: November 18, 2020